Atmos. Meas. Tech., 2, 177–191, 2009
www.atmos-meas-tech.net/2/177/2009/

Atmospheric Measurement Techniques

Retrieval of SO_2 from thermal infrared satellite measurements: correction procedures for the effects of volcanic ash

S. Corradini[1], **L. Merucci**[1], **and A. J. Prata**[2]

[1]Istituto Nazionale di Geofisica e Vulcanologia,Via di Vigna Murata 605, 00143 Roma, Italy
[2]Norwegian Institute for Air Research, Instituttveien 18 Kjeller, 2027, Norway

Received: 21 November 2008 – Published in Atmos. Meas. Tech. Discuss.: 9 February 2009
Revised: 12 May 2009 – Accepted: 13 May 2009 – Published: 26 May 2009

Abstract. The simultaneous presence of SO_2 and ash in a volcanic plume can lead to a significant error in the SO_2 column abundance retrieval when multispectral Thermal InfraRed (TIR) data are used. The ash particles within the plume with effective radii from 1 to 10 μm reduce the Top Of Atmosphere (TOA) radiance in the entire TIR spectral range, including the channels used for SO_2 retrieval. The net effect is a significant SO_2 overestimation.

In this work the interference of ash is discussed and two correction procedures for satellite SO_2 volcanic plume retrieval in the TIR spectral range are developed to achieve an higher computational speed and a better accuracy.

The ash correction can be applied when the sensor spectral range includes the 7.3 and/or 8.7 μm SO_2 absorption bands, and the split window bands centered around 11 and 12 μm required for ash retrieval. This allows the possibility of simultaneous estimation of both volcanic SO_2 and ash in the same data set. The proposed ash correction procedures have been applied to the Moderate Resolution Imaging Spectroradiometer (MODIS) and the Spin Enhanced Visible and Infrared Imager (SEVIRI) measurements. Data collected during the 24 November 2006 Mt. Etna eruption have been used to illustrate the technique. The SO_2 and ash estimation is carried out by using a best weighted least squares fit method and the Brightness Temperature Difference (BTD) procedures, respectively. The simulated TOA radiance Look-Up Table (LUT) needed for the SO_2 column abundance and the ash retrievals have been computed using the MODTRAN 4 Radiative Transfer Model.

The results show the importance of the ash correction on SO_2 retrievals at 8.7 μm, where the corrected SO_2 column abundance values are less than 50% of the uncorrected values. The ash correction on SO_2 retrieval at 7.3 μm is much less important and only significant for low SO_2 column abundances. Results also show that the simplified and faster correction procedure underestimates the ash correction compared with the more time consuming but more accurate correction procedure. Such underestimation is greater for instruments having better ground pixel resolution, i.e. greater for MODIS than for SEVIRI.

Correspondence to: S. Corradini
(corradini@ingv.it)

1 Introduction

Volcanic eruptions are by their nature unpredictable and can send large amounts (Tg) of gas and particles high into the troposphere and sometimes into the stratosphere. Volcanic clouds contain a mix of silicate-bearing ash particles in the size range 0.1 μm to mm size or larger and gases, principally H_2O, CO_2, SO_2 and HCl. Interest in determining the abundances of these gases and also determining the microphysics of ash particles is high because of their effects on the environment (Thordarsson and Self, 2003), including the effects on climate (Robock, 2000), on public health (Horwell and Baxter, 2006) and because of the dangers of these substances to aviation (Casadevall, 1994). Satellites are useful for measuring volcanic clouds because of the large vertical range of these emissions and their likely large horizontal spread. Also, since volcanoes are globally distributed and inherently dangerous, satellite measurements offer a practical and safe platform from which to make observations.

Over recent years methods for deriving microphysical properties of volcanic clouds using satellite data have demonstrated that quantitative information of both ash and gas (SO_2) can be retrieved (Wen and Rose, 1996; Prata and

Grant, 2001). These methods generally rely on using data in the infrared window region between 7–14 μm to determine column abundance of SO_2 and infrared optical depth, particle radius and mass concentration for ash particles.

The first types of satellite measurements of volcanic clouds used visible imagery to infer the spatial extent and movement of clouds. Infrared window (7–14 μm) measurements were used to derive cloud top temperatures and then cloud top height by assuming the clouds to be opaque and by using a nearby radiosonde measurement of the change of atmospheric temperature with height. With improvements in satellite instruments (more spectral channels, better accuracy and spatial resolution) it was demonstrated that two infrared channels centered near 11 and 12 μm could be used to uniquely identify silicate-bearing ash (Prata, 1989a, b). Further work (Wen and Rose, 1994; Prata and Grant, 2001) showed that by utilizing microphysical and radiative transfer models it was possible to retrieve fine-ash (1–10 μm, radius) particle size, optical depth and subsequently mass concentrations.

SO_2 is an important volcanic gas because of its effects on the environment (e.g. acid rain, effects on plants and public health) and also because once it has reached high altitudes (>6 km) it can be transported over long distances, has a greater residence time and can be oxidized to form sulphates. The sulphates are capable of reflecting solar radiation and causing surface cooling (Robock, 2000). While it is well known that volcanic ash particles can have a deleterious effect on aircraft engines, the effects of SO_2 and sulphates on aircraft are not well understood. However, as SO_2 and ash are often emitted by an erupting volcano simultaneously, and as the winds can transport these substances together, a measurement of SO_2 can be used, in some circumstances, as a proxy for ash. This is particularly important for aviation, when the volcanic debris has been transported over long distances and the satellite-based ash detection signal is weak.

Progress on measuring volcanic gases from satellite measurements has been restricted mostly to SO_2 using ultraviolet and infrared measurements (e.g. Krotkov et al., 2006) and HCl using microwave measurements (Waters et al., 2006). Methods for determining SO_2 from satellite instruments are now quite mature and these measurements can be made with greater precisions and accuracies than those for volcanic ash. In this work we concentrate only on the infrared retrieval methods for SO_2 with the aim of improving the algorithms and an eventual goal of achieving accuracies comparable to those from using ultra-violet sensors (e.g. OMI and GOME-2).

There are three regions of the IR spectrum where SO_2 has strong absorption: 4.0, 7.3 and 8.7 μm. The absorption in the 4.0 μm region is weak and the retrieval is complicated by reflected solar radiation during the day. The 7.3 μm feature is the strongest SO_2 absorption, but retrieval in this regions is complicated by absorption and emission from water vapour (Prata et al., 2003). The feature at 8.7 μm is potentially the most useful because it lies within the atmospheric window where absorption by other gases, principally water vapour, is least. However, volcanic ash also absorbs radiation throughout the window region and there is likely to be interference between the absorption by ash and absorption by SO_2. Realmuto et al. (1994), Watson et al. (2004) and Pugnaghi et al. (2005) have shown that this region can be used to infer SO_2 from volcanoes emitting low-level plumes, as well as SO_2 in violent eruptions which may also contain copious amounts of ash.

This paper addresses the issue of accurately determining the column abundance of SO_2 within a volcanic cloud by utilizing thermal infrared satellite measurements. In particular the focus of this work is to investigate the effect of ash on the retrieval of SO_2 in the 7.3 and 8.7 μm wavelength regions.

The paper is organized as follows: in Sect. 2 the motivation of the work is discussed. In Sect. 3 an overview of the SO_2 and ash retrieval schemes is presented and in Sect. 4 the ash correction procedures are described. Section 5 provides a description of the MODIS and SEVIRI satellite instruments used to make the measurements, illustrated in the test cases. We summarize our findings in Sects. 6 and 7.

2 Motivation of the work

During volcanic eruptions ash and SO_2 can be emitted simultaneously. The plume ash particles (from 1 to 10 μm) tend to reduce the Top Of Atmosphere (TOA) radiance in the entire TIR spectral range (7–14 μm), including the channels used for the SO_2 retrieval. The result is a significant SO_2 column abundance overestimation. Figure 1 shows the comparison between the TOA background radiance (blue line), the TOA radiance computed considering a volcanic SO_2 plume with 5 g m^{-2} (green line) and the TOA radiance considering a plume containing both SO_2 (5 g m^{-2}) and ash (Aerosol Optical Thickness AOT=1 and effective radius r_e=2.34 μm) (red line). All the simulations have been performed using the MODTRAN 4 Radiative Transfer Model (RTM) (Berk et al., 1989; Anderson et al., 1995) considering a surface temperature and emissivity of 292 K and 0.99, respectively, a plume-top altitude of 5000 m and a plume thickness of 1000 m. The other curves plotted are the MODIS-Aqua TIR response functions; the yellow and purple lines represent the bands used for the SO_2 and ash retrieval respectively.

As Fig. 1 shows, the presence of ash produces a significant radiance decrease not only in 10–13 μm spectral range, but over all the TIR spectral range and in particular on the 8.7 μm channel. The same observations can be made by analyzing the Fig. 2 that shows the radiance percentage differences convolved with the MODIS-Aqua response functions – the percentage radiance is computed considering the TOA background radiance and the TOA radiance of a volcanic SO_2'plume for different values of SO_2 column abundance (top plate), and the TOA radiance of a volcanic ash

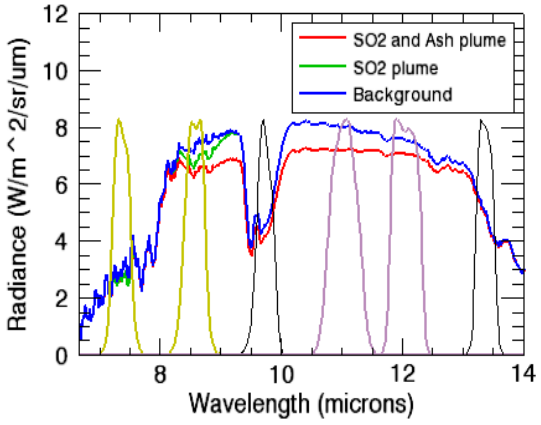

Fig. 1. Comparison between TOA background radiance (blue line), TOA radiance considering a volcanic plume with 5 g m^{-2} of SO_2 (green line) and TOA radiance considering a plume with both SO_2 (5 g m^{-2}) and ash (AOT=1 and r_e=2.34 μm) (red line). The near-Gaussian curves represent the MODIS-Aqua TIR response functions: the yellow and purple lines are the channels used for SO_2 and ash retrievals respectively. All the simulations have been carried out using MODTRAN RTM and considering the surface temperature and emissivity at 292 K and 0.99 respectively with a plume top altitude of 5000 m and plume thickness of 1000 m.

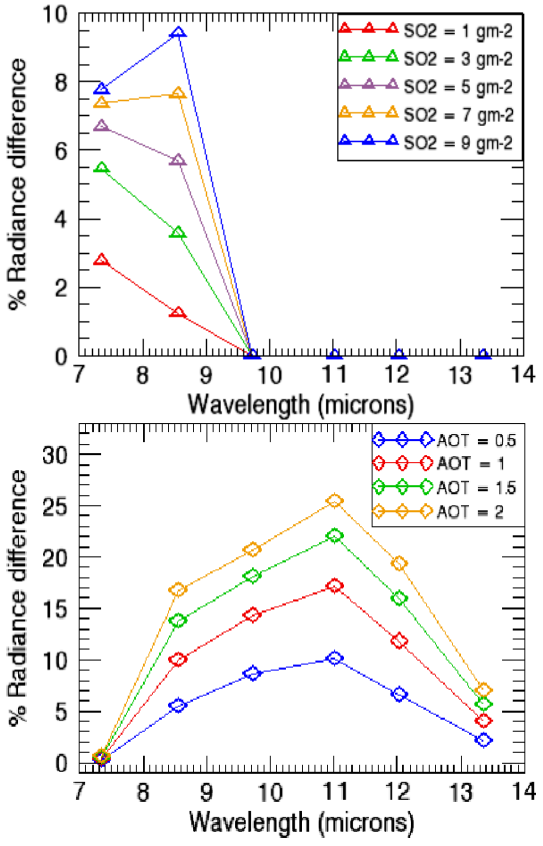

Fig. 2. TOA radiance percentage difference convoluted with TIR MODIS-Aqua response functions. Top plate: TOA radiance percentage difference between TOA background radiance and TOA radiance computed considering a volcanic plume with different values of SO_2 column abundances. Bottom plate: TOA radiance percentage difference between TOA background radiance and TOA radiance computed considering a volcanic ash plume with r_e=2.34 μm for different values of AOT. All the simulations have been carried out considering the surface temperature and surface emissivity at 292 K and 0.99 respectively with a plume top altitude of 5000 m and plume thickness of 1000 m.

plume for different values of AOT (assuming r_e=2.34 μm) (bottom plate). Comparing the top and bottom plates it can be seen that the radiance percentage difference variation on the 8.7 μm channel with AOT=0.5 is comparable to the percentage difference for an SO_2 column abundance variation of 5 g m^{-2}. At 8.7 μm an ash plume with r_e=2.34 μm and AOT=0.5 produces the same TOA radiance variation as an SO_2 plume with 5 g m^{-2}. The effect of ash at 7.3 μm is much less important and the radiance percentage difference results are always less than 3% for all the simulations considered. Therefore the ash correction can produce effects only for low SO_2 column abundance values.

In this work two different procedures for SO_2 volcanic plume retrieval in the TIR spectral range have been developed in order to correct for the effect of ash. The two procedures address the requirements of high speed of computation (*meanval-procedure*) and of accuracy (*pixval-procedure*). The ash corrections have been applied to MODIS and SEVIRI measurements collected during the November 2006 Mt. Etna volcanic eruption.

3 Retrieval schemes

3.1 SO_2 retrieval

In the TIR spectral range, SO_2 has two wide absorption bands centered around 7.3 and 8.7 μm (see top plate of Fig. 3). Due to the strong presence of atmospheric water vapour (see bottom plate of Fig. 3) the 7.3 μm band is generally used when the volcanic plumes rise over 3–4 km, i.e. above the most of the water vapour. The 8.7 μm channel lies in a relatively transparent region and can be used to retrieve SO_2 in the lower troposphere. The 8.7 μm SO_2 retrieval scheme has been described by Realmuto et al. (1994), Watson et al. (2004) and Pugnaghi et al. (2005) respectively for TOMS, MODIS and ASTER, while the 7.3 μm retrieval procedure was described by Prata et al. (2003) for the TOVS/HIRS sensors, and by Prata and Bernardo (2007) for the high spectral resolution AIRS sounder.

In this work the SO_2 column abundance, on both the 7.3 and 8.7 μm channels is retrieved from a pixel-by-pixel best weighted least squares fit procedure using satellite sensor

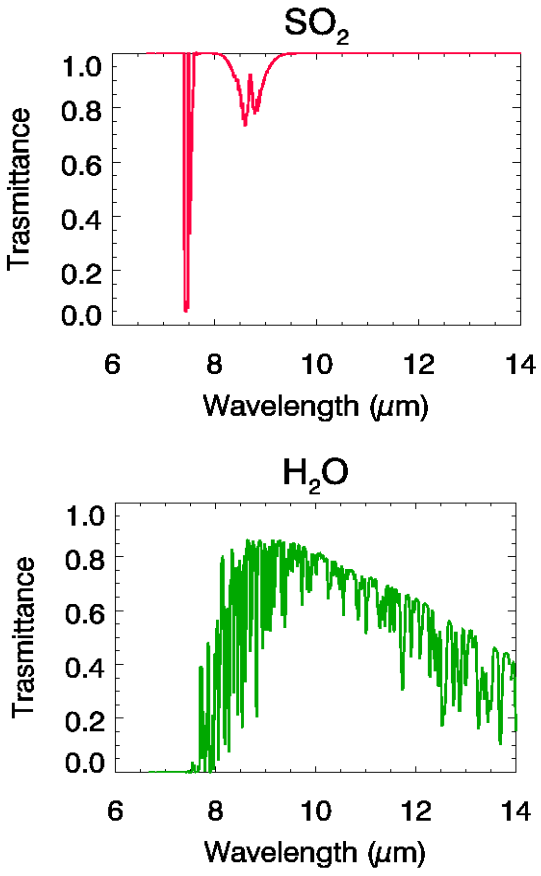

Fig. 3. The top and bottom plots show, respectively, the SO_2 and the water vapour transmittance in the TIR spectral range.

measurements and simulated radiances. The function being minimized may be written,

$$\chi^2_{c_s}(n,\,m) = \sum_{j=1}^{k} \left[\frac{R^{(n,\,m)}_{M,\,j} - R_{S,\,j}(c_s)}{R^{(n,\,m)}_{M,\,j}} \right]^2 w_j \qquad (1)$$

where:
k is the number of channels (j) used for the minimization;
$R^{(n,\,m)}_{M,\,j}$ is the j-th channel measured radiance for the pixel $(n,\,m)$;
$R_{S,\,j}(c_s)$ is the j-th channel simulated radiance varying the SO_2 column abundance c_s;
w_j is the j-th channel weight.
The SO_2 retrieval error has been also estimated computing the instrumental radiance variation for each channel $\Delta R_{M,\,j}$ due to the $NE\Delta T$, perturbing the 7.3 and 8.7 μm instrumental radiances by $\pm\Delta R_{M,\,j}$ values, and re-doing the SO_2 retrieval. The variation from the unperturbed result has been assumed as the SO_2 total mass retrieval uncertainty.

The simulated radiances are computed by using MODTRAN 4 Radiative Transfer Model (RTM) (see Sect. 3.3).

3.2 Ash detection and retrieval

Ash detection is carried out by using the Brightness Temperature Difference (BTD) procedure (Prata, 1989a, b) applied to channels centered around 11 and 12 μm while effective radius and aerosol optical thickness at 0.55 μm have been retrieved from the "inverted arches" of the BTD vs. brightness temperature at 11 μm curves by varying AOT and r_e (Wen and Rose, 1994; Prata and Grant, 2001; Yu et al., 2002; Ellrod et al., 2003). To take into account the atmospheric water vapour absorption in the 11–12 μm spectral range, a water vapor correction procedure has also been applied (Corradini et al., 2008). Using the AOT and r_e retrievals, the pixel-by-pixel mass is computed by using the simplified formula suggested by Wen and Rose (1994),

$$M(n,\,m) = \frac{4}{3} \frac{S\rho r_e^{(n,\,m)} \mathrm{AOT}^{(n,\,m)}}{Q_{\mathrm{ext}}\left(r_e^{(n,\,m)}\right)} \qquad (2)$$

where:
S is the pixel surface;
ρ is the particle density;
$r_e^{(n,\,m)}$ is the effective radius of pixel $(n,\,m)$;
$\mathrm{AOT}^{(n,\,m)}$ is the aerosol optical thickness of pixel $(n,\,m)$;
$Q_{\mathrm{ext}}(r_e^{(n,\,m)})$ is the extinction efficiency factor at effective radius $r_e^{(n,\,m)}$.
Also in this case, the simulated radiances needed for the ash retrievals have been computed using the MODTRAN RTM (see the next section).

3.3 Look-up table generation

The simulated TOA radiances Look-Up Table (LUT) used for both SO_2 and ash retrievals derives from the MODTRAN 4 RTM. The simulations have been performed using as input the atmospheric profiles (pressure, temperature and humidity), the surface characteristics (temperature and emissivity), the plume geometry (plume altitude and thickness) and the volcanic ash optical properties. The ash optical properties (single scattering albedo, extinction coefficient and asymmetry parameter) have been computed using the Mie code developed by the Earth Observation Data Group (EODG) of the Atmospheric Oceanic and Planetary Physics Department (Oxford University). Because of the lack of information about the characteristics of the ash emitted by the volcano, the andesite refractive index (Pollack et al., 1973) and a log-normal distribution (width (σ)=1.77, minimum and maximum radii corresponding to $\pm 3\sigma$ from the central wavelength) have been considered as reasonable choices. The TOA radiance LUT are computed for 21 values of SO_2 column abundance (from 0 to 10 g m^{-2}, step 0.5 g m^{-2}), 21 values of aerosol optical thickness (from 0 to 10 in steps of 0.5) and 8 values of effective radii (from 0.4 to 10 μm, with a constant step in a logarithmic scale). This gives a total of 3528 simulations ($R_{S,\,i}\,(c_s,\,\mathrm{AOT},\,r_e)$).

4 Ash correction procedures

The ash correction procedures for the SO_2 column abundance retrieval consist of three different steps:

1) SO_2 column abundance and ash are retrieved simultaneously and independently. The SO_2 column abundance maps at 7.3 and 8.7 μm, the aerosol mass, AOT and r_e maps, and also the mean values of AOT and r_e of the plume are retrieved. In this step, the SO_2 retrievals are obtained while not considering the influence of ash on these channels, i.e. using the terms $R_{S,i}(c_s, 0, 0)$ for the simulated TOA radiances.

2) The plume pixels containing both SO_2 and ash are identified by the intersection between the ensembles of pixels where SO_2 and ash have been detected.

3) The SO_2 retrieval on both 7.3 and 8.7 μm channels is carried out again only for the SO_2 and ash intersection ensemble of pixels.

The *meanval-procedure* uses the radiances computed by interpolation of the mean aerosol optical thickness ($\overline{\mathrm{AOT}}$) and mean effective radius ($\overline{r_e}$) as simulated radiances, i.e. using the terms $R_{S,i}(c_s, \overline{\mathrm{AOT}}, \overline{r_e})$) as simulated TOA radiances. The AOT and r_e averages have been computed considering all the ash pixels detected in Step 1.

The *pixval-procedure* uses as simulated radiances the radiances computed by interpolation of the aerosol optical thickness ($\mathrm{AOT}^{(n,m)}$) and effective radius ($r_e^{(n,m)}$) for each identified pixel (n, m), i.e. using as simulated TOA radiances the terms $R_{S,i}(c_s, \mathrm{AOT}^{(n,m)}, r_e^{(n,m)})$.

The *meanval-procedure* is faster because the interpolation is computed once for all pixels, while using the *pixval-procedure* the interpolation is computed for each pixel; for this reason the latter procedure results are more accurate.

5 Satellite instruments and data set

The satellite sensors for which the ash correction procedure can be applied are those having the 7.3 and/or 8.7 μm SO_2 absorption channels, and the channels centered around 11 and 12 μm used for the ash retrievals. In this work the ash correction procedures have been applied to the TIR images of the MODIS and SEVIRI instruments collected over Mt. Etna volcano during the November 2006 eruption.

5.1 MODIS

MODIS is a multispectral instrument with 36 spectral bands in the wavelength range from visible to thermal infrared. MODIS is aboard the NASA Terra and Aqua polar satellites, launched in 1999 and 2002 respectively, as part of the Earth Observing System (EOS) mission (Barnes et al., 1998; http://modis.gsfc.nasa.gov/). Terra's descending node (from north to south) crosses the equator in the morning at about 10:30 a.m. (local time), while the Aqua ascending node (south to north) crosses the equator at about 1:30 p.m. (local time). MODIS has a spatial resolution of 1000 m at nadir for the TIR bands used in our study. Bands 28 and 29 centered around 7.3 and 8.7 μm are used for the SO_2 column abundance retrieval while bands 31 and 32, centered around 11 and 12 μm, are used for the ash detection and retrievals. The Noise Equivalent Temperature Difference ($NE\Delta T$), is 0.05 K (at 300 K) for all SO_2 and ash bands except for the channel 28 (7.3 μm band), which is 0.25 K (at 250 K) (http://modis.gsfc.nasa.gov/). The sensor scans $\pm 55°$ across-track about the nadir from the EOS orbit altitude of 705 km, resulting in a 2330 km swath and full global coverage every one to two days.

5.2 SEVIRI

SEVIRI is the main sensor of the Meteosat Second Generation (MSG) satellite. The MSG platform is a geosynchronous satellite launched on 28 August 2002 (http://www.eumetsat.int). The orbit altitude is 42 000 km (measured from the center of the Earth) with a period of 24 h and a nadir point of approximately 3° W over the Equator. SEVIRI is a 50 cm diameter aperture, line-by line scanning radiometer which provides images data in four Visible and Near InfraRed (VNIR) channels and eight infrared (IR) channels. The VNIR channels include the High Resolution Visible (HRV) channel which contains 9 broadband detection elements to scan the Earth with 1 km of spatial resolution. All the other channels (including the IR channels) are designed with 3 narrow band detection elements per channel, to scan the Earth with a 3 km spatial resolution at nadir. Its main advantage is the repeat cycle of 15 min, which includes on board calibration time, the retrace and the overall satellite stabilization process. Bands 6 and 7 (centered around 7.3 and 8.7 μm) and bands 9 and 10 (centered around 10.8 and 12 μm) are used for the SO_2 and ash retrievals, respectively. The $NE\Delta T$ varies from 0.11 K (bands 7 and 9) to 0.16 K (bands 6 and 10) at the reference temperature of 300 K, except for band 6 where it is measured at 250 K. SEVIRI's characteristics allow high temporal resolution retrievals, which are very useful in the study of the evolution of volcanic plumes.

5.3 Test Case measurements

Mt. Etna is located in the eastern part of Sicily (Italy) (see Fig. 4) and is one the major degassing volcanoes in the world (Allard et al., 1991). Etna's general quiescent state is periodically interrupted by eruptive crises, during which significant SO_2 and ash emissions can reach the area surrounding the volcano, causing problems to the population of the region (Andronico et al., 2005) and to air traffic (Catania and Reggio Calabria airports are nearby). During 2006 Mt. Etna exhibited episodic explosive activity producing SO_2 and ash plumes that rose up into the atmosphere and drifted several km away from the vent. These episodes occurred frequently from September to December (Spinetti et al., 2006; De Beni

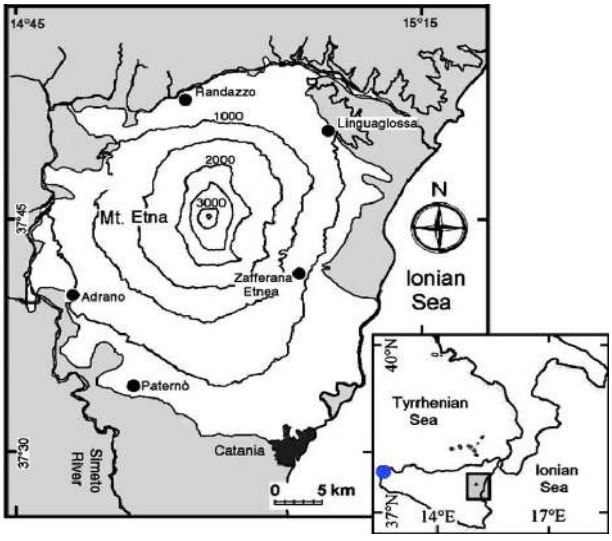

Fig. 4. The Mt. Etna volcano, Sicily (Italy) (37.734° N, 15.004° E, 3330 m a.s.l.) is located in the eastern part of Sicily. The Trapani WMO station (37.928° N, 12.508° E, 14 m a.s.l.) on the western tip of Sicily is indicated by a blue-colored point. The atmospheric profiles used for the MODTRAN simulations were obtained from this site.

et al., 2006) showing weak intensity and short duration compared to previous 2001 and 2002 eruptions (Andronico et al., 2005; Behncke et al., 2003). The 24 November 2006 SO_2 and ash emission started at about 04:00 and 09:00 UTC respectively and ended simultaneously at about 15:00 UTC. The eruption took place both at the summit and the south east crater of Mt. Etna and produced the largest volume of ash in the entire September–December eruptive period. On this day the wind was blowing from the NNW direction causing the ash plume to move towards the city of Catania. The ash fallout created major problems for the Fontanarossa International Airport of Catania which was subsequently closed to air traffic. In this work the SEVIRI and MODIS images collected on 24 November at 12:15 and 12:20 UTC respectively are considered as a test case. Figure 5 shows the RGB and channel 11 μm images (left and right plates) for MODIS and SEVIRI (top and bottom plates) instruments.

6 Results and discussion

In this section the characteristics of the MODTRAN simulations and the details of the ash correction procedures applied to the MODIS and SEVIRI measurements are presented.

6.1 Characteristics of MODTRAN simulations

As described in Sect. 3.3 the simulated TOA radiances have been performed using as input the atmospheric profiles, the plume geometry, the surface characteristics, and the ash optical properties. The 24 November 2006 atmospheric vertical profiles derived from Trapani WMO Meteo station (the nearest WMO station to the Etnean area) were measured at 12:00 UTC. The plume-top altitude is estimated by comparing the ash plume top temperature, computed as the mean brightness temperature of channels centered around 11 and 12 μm of the most opaque plume region (near the vent), and the Trapani radiosounding temperature profile. The procedure gives a plume-top height of about 5000 m which is consistent with independent observations (Spinetti et al., 2006). The plume thickness has been assumed to be 1000 m. For both of the images, the processing has been applied only over the sea. The sea surface emissivity was estimated from a convolution between the ASTER spectral emissivity library database (http://speclib.jpl.nasa.gov/) and the MODIS and SEVIRI response functions. The convolution gives the same emissivity values for both instruments (see Table 1). The sea surface temperature has been retrieved by inversion of the radiative transfer equation in the TIR spectral range, using the channels centered around 11 and 12 μm. The volcanic plume is not transparent in these channels, therefore the surface temperature estimation under the plume is not possible. The sea surface temperature below the plume has been assumed as the mean temperature of two wide regions selected just outside the plume area (see Corradini et al., 2008). The mean sea surface temperature retrieved for both MODIS and SEVIRI is 291.5 K$\pm$1 K.

Table 1. Spectral sea surface emissivity used for MODIS and SEVIRI retrievals.

Central Wavelength (μm)	Sea Surface Emissivity
7.3	0.982
8.7	0.984
11	0.990
12	0.986

6.2 MODIS image elaboration

6.2.1 First step: ash and SO_2 retrievals

In the first step the simultaneous retrieval of SO_2 and ash is carried out. The SO_2 retrieval is obtained without considering the influence of ash on MODIS channels 28 and 29. Figure 6 shows the ash (top plates) and SO_2 (bottom plates) retrievals using MODIS data. The top left and top right plates show the ash aerosol optical thickness at 0.55 μm and the effective radius maps, while the bottom left and bottom right plates show the SO_2 retrievals at 7.3 and 8.7 μm respectively. The top left plate shows that larger AOT occur in the area close to the vent, while the smaller values occur at the cloud edges. There are also other regions of

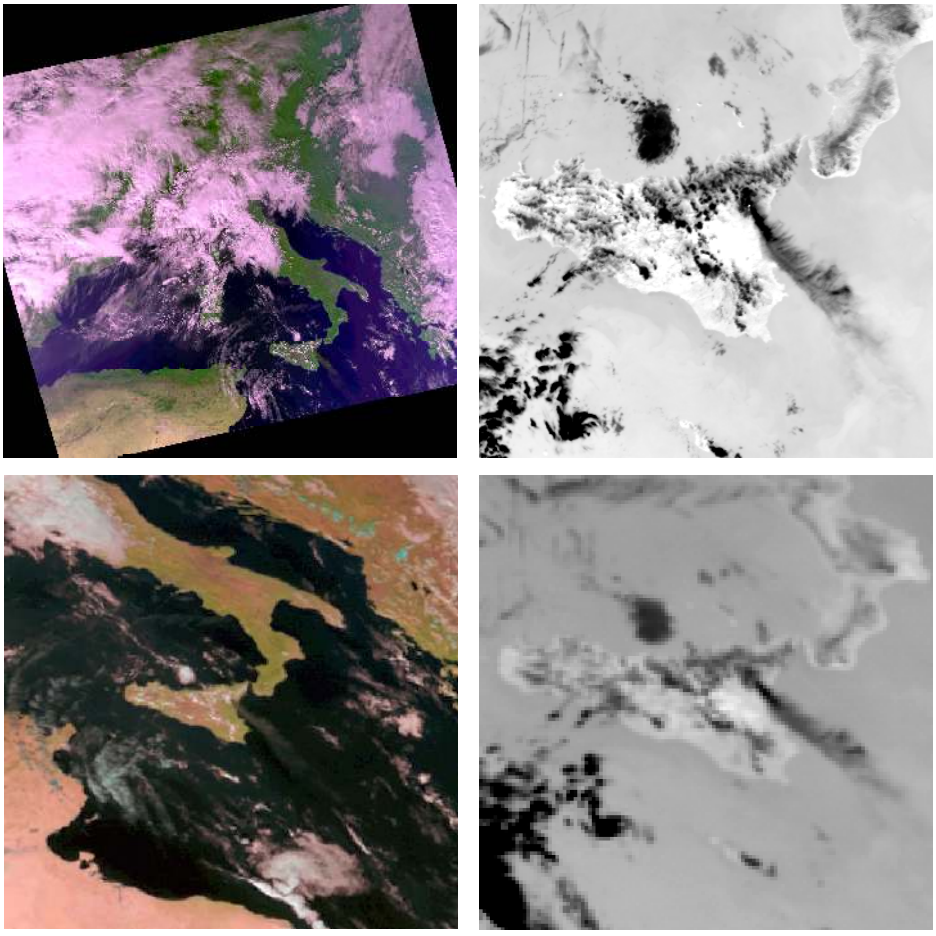

Fig. 5. Top: 24 November 2006 MODIS-Aqua image (12:20 UTC). Bottom: 24 November 2006 SEVIRI image (12:15 UTC). The left plates show an RGB composition while the right plates show the 11 μm channel images zoomed on Etnean area.

high AOT probably due to volcanic puffs. The particle effective radii (top right plate) are distributed non-uniformly along the plume: larger particles (up to 5 μm) thicken around the western part of the plume. The total mass, mean AOT and mean effective radius are: 3805 tons, 0.31 and 3.06 μm respectively. Figure 7 shows the AOT and r_e histograms and mean values. The SO_2 column abundance maps indicate a meaningful underestimation of the 7.3 μm retrieval compared to the 8.7 μm retrieval, the total masses computed are: 1017 and 22 660 tons, respectively. The main reason of the SO_2 differences between 8.7 μm and 7.3 μm retrievals is due to the atmospheric water vapour absorption that is much stronger around 7.3 μm. In case of tropospheric eruptions, at this wavelength the water vapour tends to override the plume signal making the SO_2 retrieval critical and meaningfully underestimated (see Sect. 3.1).

Using the procedure described in Sect. 4 the results show a SO_2 total mass retrieval uncertainty of 40% and 3% for 7.3 μm and 8.7 μm, respectively (see Table 2). In this case of tropospheric eruption, the 7.3 μm SO_2 retrieval uncertainty result significant because the huge absorption of the atmospheric water vapour at 7.3 μm makes the radiance variation for the different SO_2 column abundances values very low, then comparable with the $\Delta R_{M,\,j}$ perturbation.

Table 2. MODIS and SEVIRI SO_2 total mass retrievals (tons) before and after ash correction.

Instrument	Before Ash Correction	Meanval Correction	Pixval Correction
MODIS (7.3 μm)	1017±610	779±470	614±246
MODIS (8.7 μm)	22 660±680	11 045±330	7195±216
SEVIRI (8.7 μm)	21 128±1270	9567±570	7371±440

The 7.3 μm MODIS SO_2 estimation has been compared with the Atmospheric Infrared Sounder (AIRS) retrieval. AIRS is a grating spectrometer operating at IR wavelengths between 3.7 and 15.4 μm (2378 channels) with a scanning of ±49° from nadir and an instantaneous field of view of 1.1° providing nadir pixels with dimensions 15×15 km^2 (Chahine

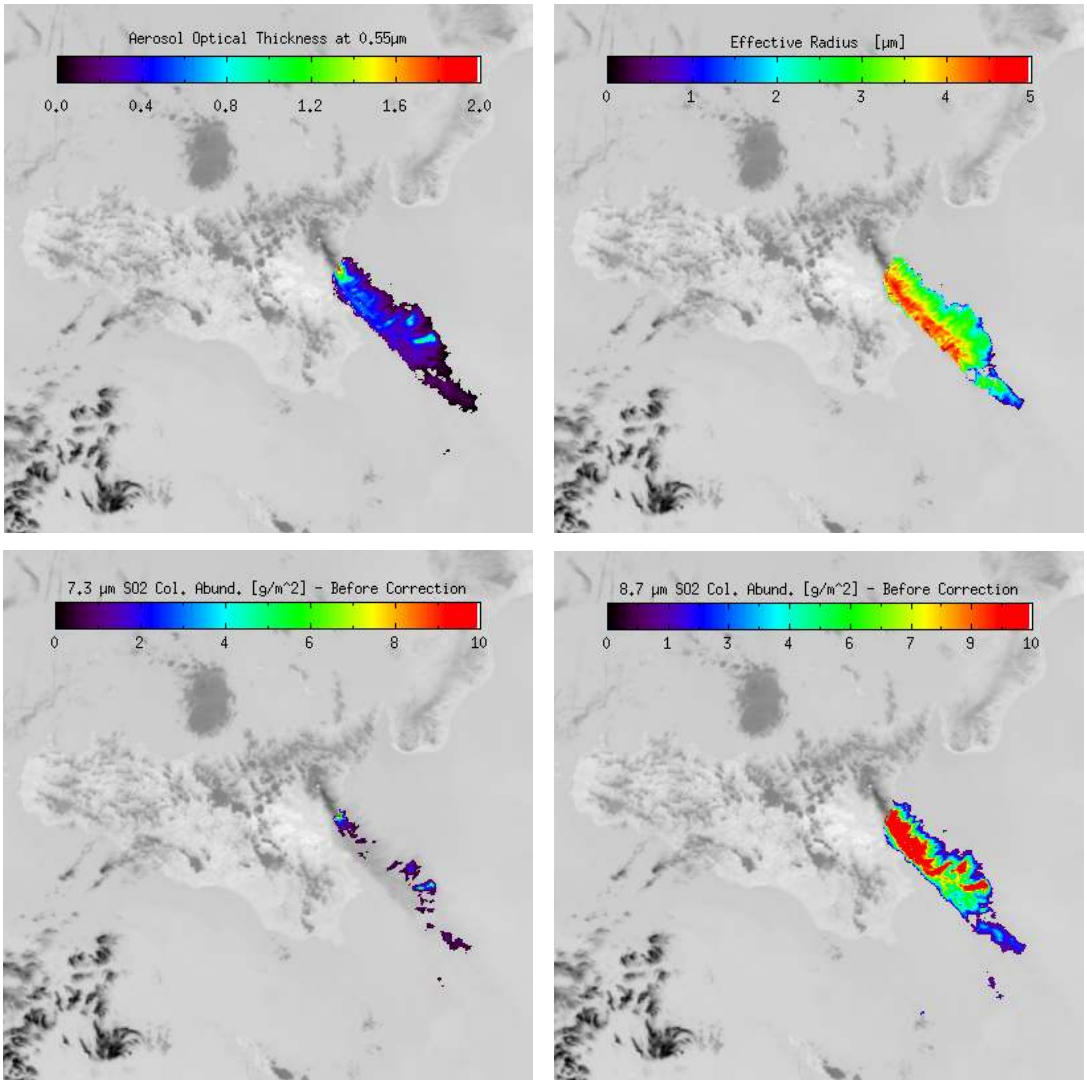

Fig. 6. 24 November 2006 MODIS image 12:20 UTC retrievals. Top left top plate: AOT at 0.55 μm; Top right plate: r_e (μm); Left bottom plate: SO_2 retrieval at 7.3 μm; Right bottom plate: SO_2 retrieval at 8.7 μm.

et al., 2006). The instrument is aboard the EOS-Aqua polar orbiting satellite. Figure 8 shows the AIRS SO_2 retrieval, using the 7.3 μm absorption band (Prata and Bernardo, 2007), for an image collected over Etna volcano on 24 November 2006 at 12:17 UTC. The SO_2 total mass retrieved by AIRS is 800 tons; this is a good match to the 7.3 μm SO_2 retrieval obtained from the MODIS data.

6.2.2 Second step: ensemble intersection

In the second step, the intersection between the SO_2 and ash maps is evaluated to obtain the ensemble of pixels containing both SO_2 and ash. The blue pixels of Fig. 9 represent pixels with ash and SO_2, while the green and red pixels are the pixels containing only ash and only SO_2, respectively.

6.2.3 Third step: ash corrections

Figure 10 shows the SO_2 retrievals (7.3 and 8.7 μm) after the ash correction using both the *meanval* and *pixval* procedures. The top and bottom plates are the 7.3 and 8.7 μm SO_2 corrected images while the top and bottom plates are the images corrected by using the *meanval-procedure* and the *pixval-procedure* respectively. The left plates show that the *meanval-procedure* tends to overestimate the correction for the pixels having AOT and r_e less than the mean values and underestimate the correction for all the other pixels. The *pixval-procedure* (right plate of Fig. 10) produces a more uniform SO_2 map. As Table 2 shows, and as expected, the correction procedure is greater at 8.7 μm than at 7.3 μm. The total mass of SO_2 retrieved at 8.7 μm is less than one half

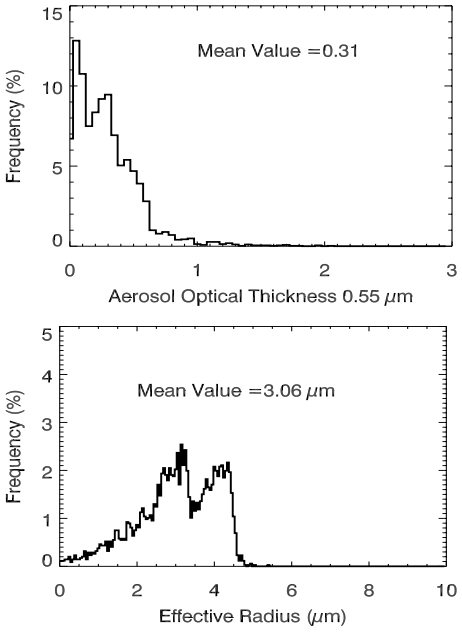

Fig. 7. 24 November 2006 MODIS image 12:20 UTC. Top plate: AOT histogram. Bottom plate: r_e histogram. The mean AOT and r_e values are also shown.

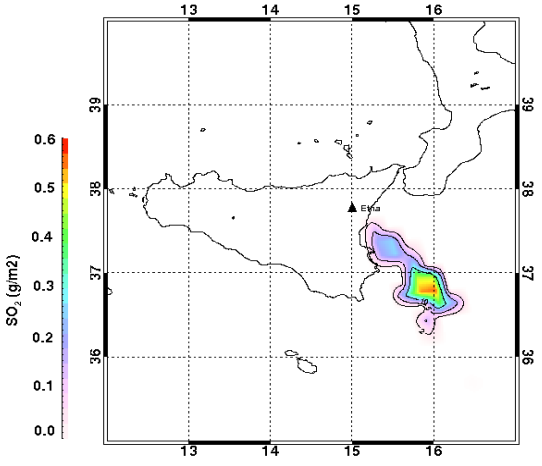

Fig. 8. AIRS SO_2 retrieval using the 7.3 μm absorption feature. The image has been recorded over Mt. Etna volcano on 24 November 2006 at 12:17 UTC.

of the total mass retrieved without correction. The variation of the total mass retrieved at 7.3 μm (see Table 2) is much less important even if the ash correction is not negligible because the SO_2 column abundance retrieved values are low (see Sect. 2). Table 2 also shows that the SO_2 total mass computed using the *pixval-procedure* is significantly lower than the total mass computed using the *meanval-procedure*. The ash correction procedures allow also to define a criterion for the identification of opaque pixels (white pixels in

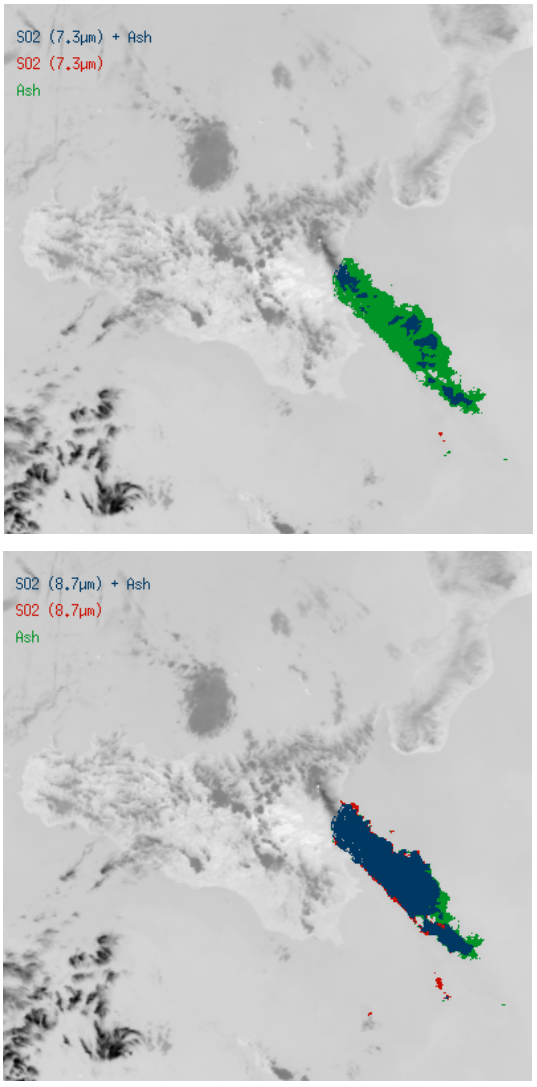

Fig. 9. 24 November 2006 MODIS image 12:20 UTC ensemble intersection. Top plate: intersection between ash and SO_2 retrieval at 7.3 μm ensembles. Bottom plate: intersection between ash and SO_2 retrieval at 8.7 μm ensembles. The blue pixels are the pixels containing both SO_2 and ash, the red and the green pixels are the pixel containing only SO_2 and only ash, respectively.

Fig. 10). For these pixels the following inequality is true,

$$R^{(n,m)}_{M,j} < \min[R^{*}_{S,j}(c_s)] \quad (3)$$

where the $R^{*}_{S,j}(c_s)$ represents the simulated radiances considering the two procedures. When the radiance measured is less than the minimum corrected simulated radiance (correspondent to the maximum values of SO_2 column abundance considered), the SO_2 retrieval is not possible. This doesn't mean that the pixel doesn't contain any SO_2, but only that the SO_2 retrieval is not well-posed. The gas/ash flux can be calculated by multiplying the integral of the column abundance,

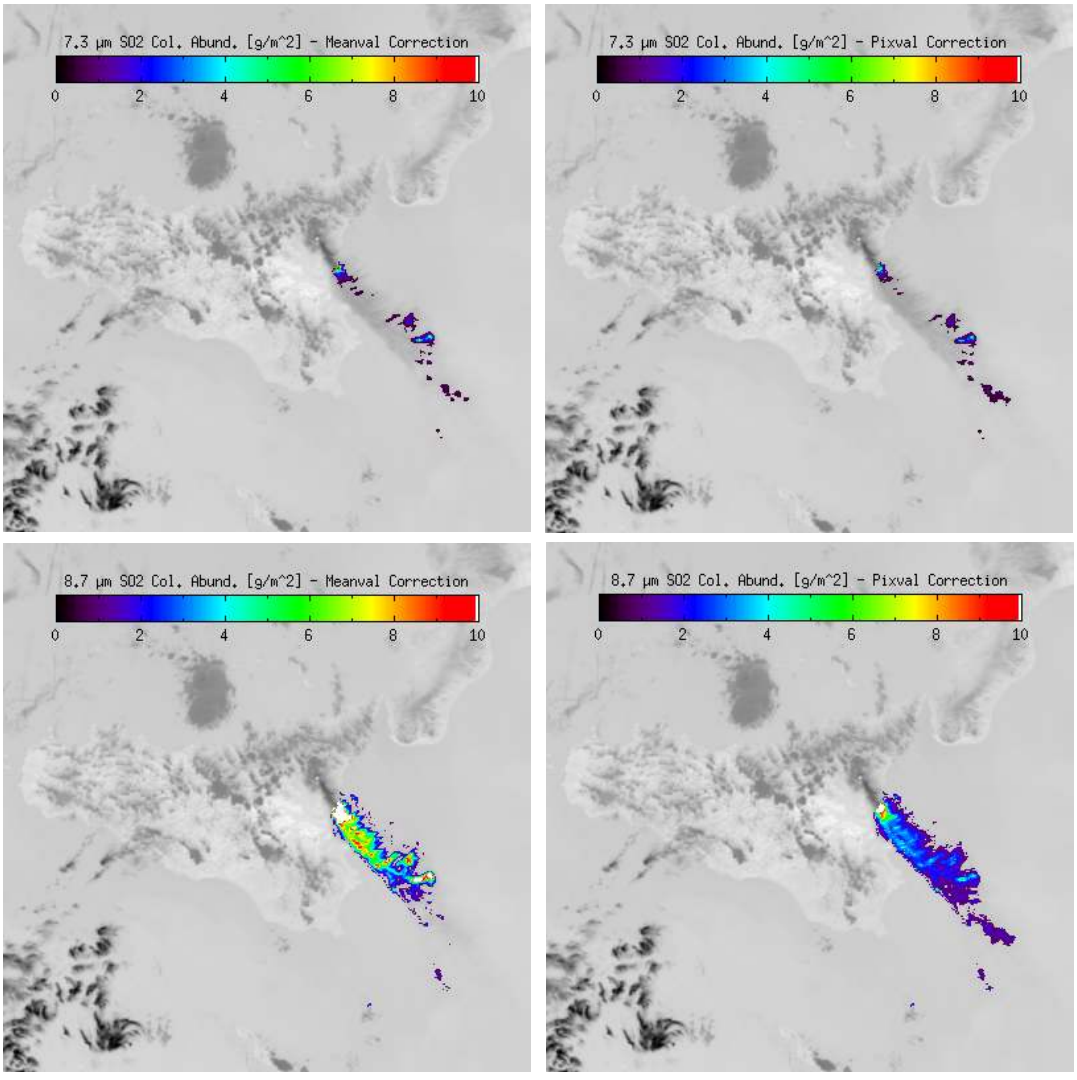

Fig. 10. 24 November 2006 MODIS image 12:20 UTC. Ash correction at 7.3 μm (top plates) and at 8.7 μm (bottom plates). The left and right plates are the images corrected by using the *meanval-procedure* and the *pixval-procedure*, respectively. The white pixels indicate the pixels where the SO_2 retrieval is not possible.

performed along each transect perpendicular to the plume axis (see small panel to the bottom right corner of Fig. 11), by the wind speed. The wind speed (6 ms^{-1}) was extracted from the Trapani atmospheric profile at the mean plume altitude (4500 m a.s.l.). Figure 11 shows the fluxes along the plume axis computed for the SO_2 retrievals at 7.3 and 8.7 μm before (pale red and pale blue lines respectively) and after the pixval ash correction (red and blue lines respectively). The green line represents the ash flux. Note in particular the big difference between the 8.7 μm SO_2 flux before and after the correction.

6.3 SEVIRI image elaboration

6.3.1 First step: ash and SO_2 retrievals

The simultaneous retrieval of SO_2 and ash is carried out and the SO_2 retrieval is obtained without considering the ash influence on SEVIRI channels 6 and 7. Figure 12 shows the ash (top plates) and SO_2 (bottom plates) retrievals using SEVIRI data: the top left and top right plates show the aerosol optical thickness at 0.55 μm and the effective radius maps, while the bottom left and bottom right plates show the SO_2 retrievals at 7.3 and 8.7 μm, respectively. Taking into account the different ground spatial resolution, the MODIS and SEVIRI ash retrievals maps (compare Figs. 12 and 6) present a good match because the same structures are identifiable

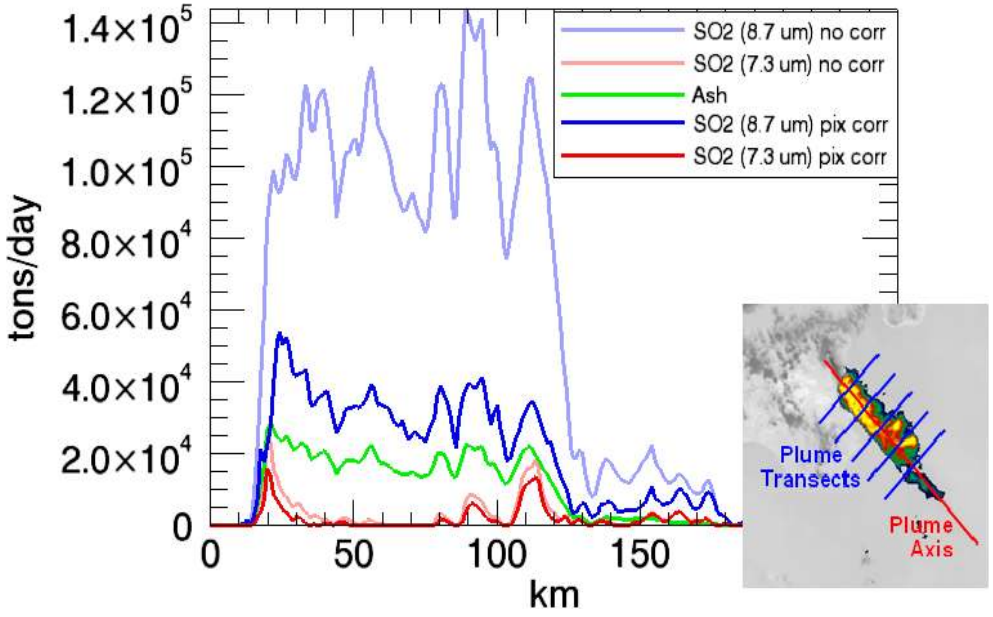

Fig. 11. SO_2 and ash flux derived from the MODIS image. The pale red and pale blue lines represents the SO_2 flux at 7.3 and 8.7 μm respectively before the correction, the red and blue lines represents the SO_2 flux at 7.3 and 8.7 μm after the pixval correction and the green line is the ash flux. The small panel, to the bottom right corner, shows the plume axis and transects definition.

(AOT and non uniform particle r_e distribution). The mean AOT (0.27), the mean r_e (3.31 μm) (see Fig. 13) and the total mass retrieved by SEVIRI (2884 tons) are in agreement with the same quantities retrieved by MODIS; all the SEVIRI values fall within the MODIS ash retrieval uncertainties (Corradini et al., 2008) estimated as 30% for mean AOT, mean r_e and 40% for the ash total mass. The 7.3 and 8.7 μm SO_2 retrieval are 57 and 21 128 tons respectively. A 40% and 6% SO_2 retrieval uncertainties have been estimated with the procedure described in Sect. 4 for 7.3 and 8.7 μm respectively. The SO_2 total mass retrieval at 8.7 μm is in agreement with the value retrieved by MODIS, while the SO_2 total mass retrieval and Fig. 12 show clearly that the procedure fails the SO_2 retrieval at 7.3 μm. In the latter case the estimated retrieval uncertainties are not enough to explain the differences between the MODIS and SEVIRI results. A deeper analysis on SEVIRI SO_2 column abundance retrieval sensitivity at 7.3 μm is needed to determine the minimum SO_2 column abundance detectable as well as the retrieval uncertainty due to the atmospheric water vapour. In this case of very low SO_2 column abundance, the radiance variation could be less than the instrument sensitivity.

6.3.2 Second step: ensemble intersection

The intersection between the SO_2 and ash maps is displayed in Fig. 14. Here again the yellow pixels represent the intersection between the sets of pixels where SO_2 and ash have been retrieved separately in step one, while the green and red pixels are the pixels containing only ash or only SO_2, respectively.

6.3.3 Third step: ash correction procedures

For all the pixels of the intersection ensemble, the SO_2 retrieval is carried out again two times, once using the *meanval-procedure* and once using the *pixval-procedure*. Figure 15 shows the SO_2 retrievals at 8.7 μm after the ash correction. The top and bottom plates are the images corrected by using the *meanval-procedure* and the *pixval-procedure*, respectively. Also in this case the SO_2 total mass at 8.7 μm is less than half of the total mass retrieved without correction (see Table 2). Table 2 highlights the fact that the SO_2 total mass computed using the *pixval-procedure* is significantly lower than the total mass computed using the *meanval-procedure*, even though the percentage difference variation due to the ash correction is lower than that computed in the MODIS data. The reason for this is that SEVIRI has a lower ground pixel resolution than MODIS. In the limit of an instrument having only one big pixel, the results of the two different procedures must be the same. Also in this case the white pixels of the Fig. 15 are the opaque pixels, identified by means of Eq. (3). The gas/ash fluxes computed along the SO_2 and ash retrieved plumes are plotted in Fig. 16. The fluxes were obtained using the same wind speed (6 ms^{-1}) as for MODIS. Note in particular the significant difference between the 8.7 μm SO_2 flux before and after the correction when ash is present.

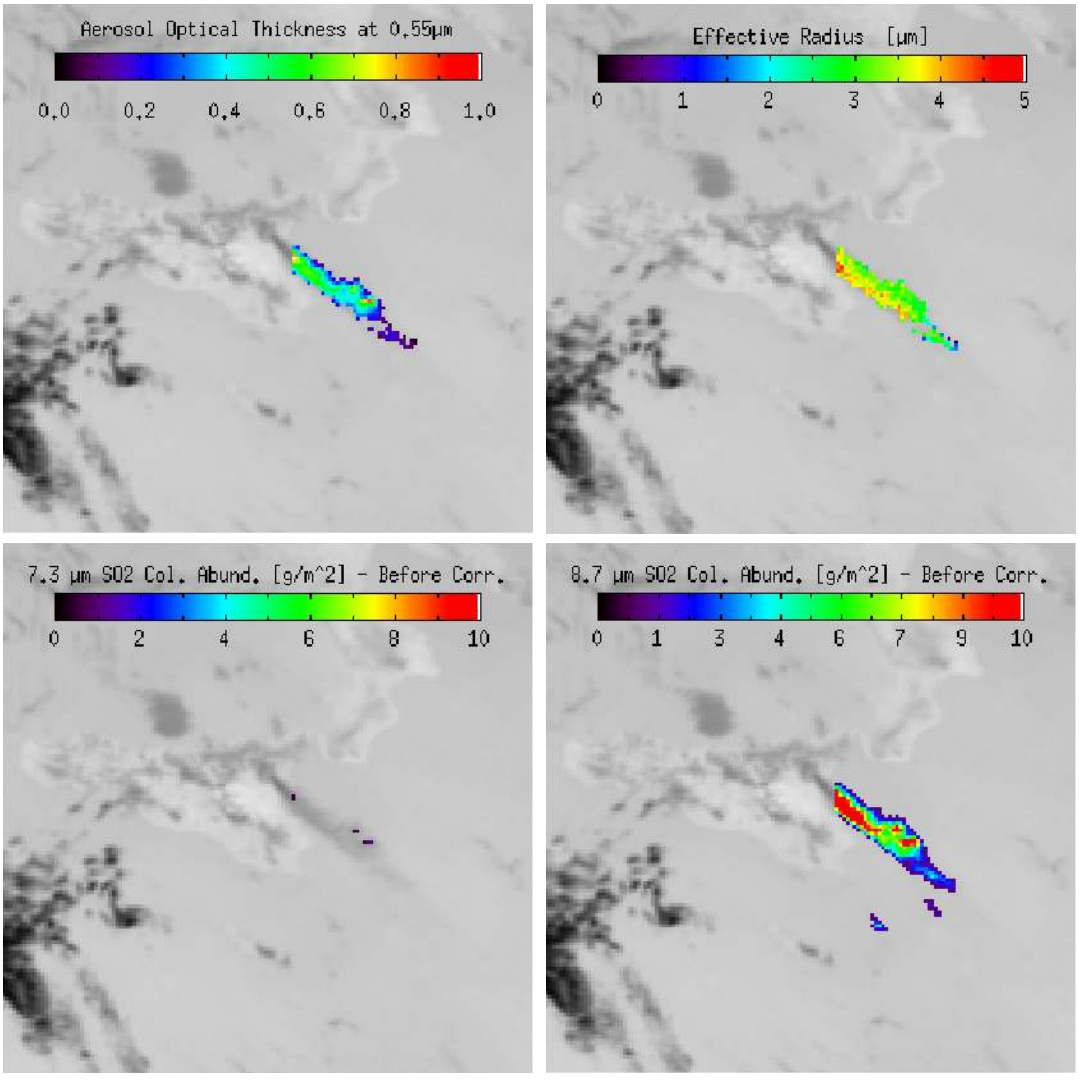

Fig. 12. 24 November 2006 SEVIRI image 12:15 UTC retrievals. Top left top plate: effective radius (μm); Top right plate: AOT at 0.55 μm. Left bottom plate: SO_2 retrieval at 8.7 μm; Right bottom plate: SO_2 retrieval at 7.3 μm.

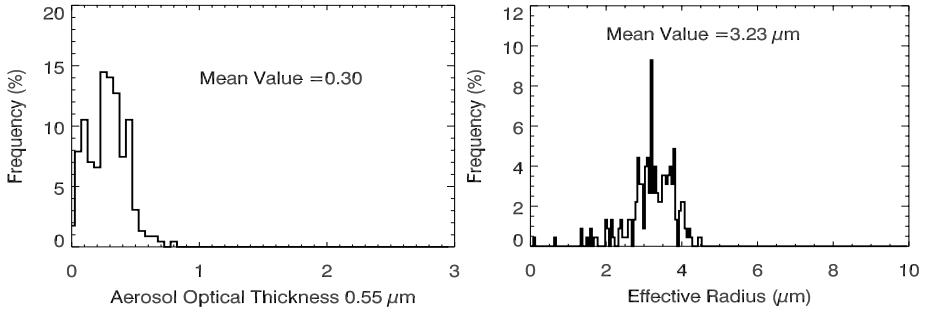

Fig. 13. 24 November 2006 SEVIRI image 12:15 UTC. Left plate: AOT histogram; Right plate: r_e histogram. The mean AOT and r_e values are also shown.

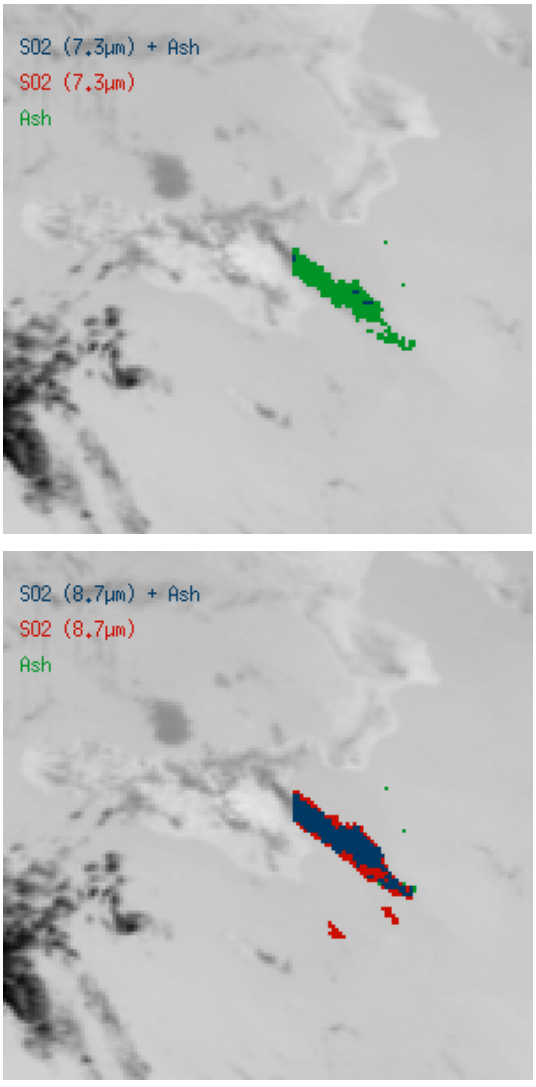

Fig. 14. 24 November 2006 SEVIRI image 12:15 UTC ensemble intersection. Top plate: intersection between ash and SO_2 at 7.3 μm ensembles. Bottom plate: intersection between ash and SO_2 at 8.7 μm ensembles.

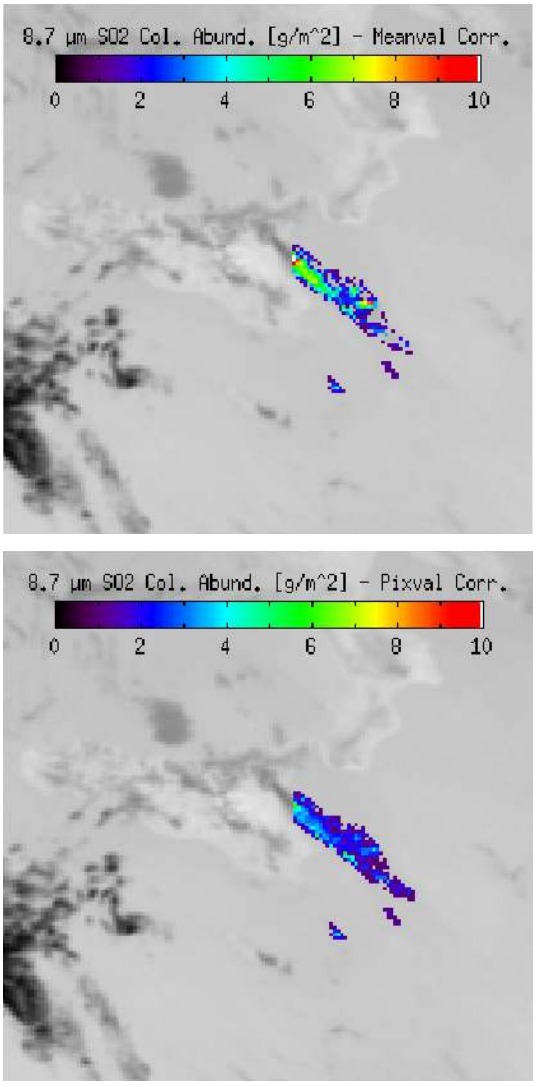

Fig. 15. 24 November 2006 SEVIRI image 12:15 UTC. Ash correction for 8.7 μm SO_2 retrieval. Top plate: meanval procedure. Bottom plate: pixval procedure.

7 Conclusions

The interference of ash on the SO_2 retrieval from TIR multispectral data of volcanic plumes has been demonstrated and analyzed. To compensate for the ash effect two correction procedures for the SO_2 retrieval have been developed. A necessary condition for the application of the procedures is a sensor spectral range that includes a channel for the SO_2 retrievals, and also the split window bands centered around 11 and 12 μm required for the ash retrieval. The two procedures satisfy the requirements of high computation speed (*meanval-procedure*) and accuracy (*pixval-procedure*) and are based on three different steps. In the first step the SO_2 column abundance and ash retrievals are computed simultaneously and independently (the SO_2 retrieval is obtained without considering the influence of ash). In the second step plume pixels containing both SO_2 and ash are identified. In the third step, only for these pixels, the SO_2 column abundance is computed again with the ash correction. The two procedures differ in this final step in considering as simulated TOA radiances, the radiance interpolated using the mean aerosol optical thickness and mean effective radius retrieved over the whole image (*meanval-procedure*), and the radiance interpolated using the aerosol optical thickness and effective radius of each identified pixel (*pixval-procedure*).

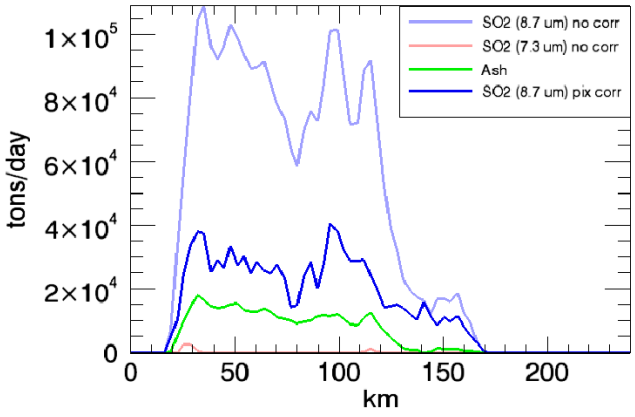

Fig. 16. SO_2 and ash flux derived from the SEVIRI image. The pale red and pale blue lines represents the SO_2 flux at 7.3 and 8.7 μm respectively before the correction, the red and blue lines represents the SO_2 flux at 7.3 and 8.7 μm after the pixval correction and the green line is the ash flux.

All the radiance simulations utilize the MODTRAN 4 RTM. Together with the ash correction, a criterion for the identification of the opaque pixels has also been described. As a test case MODIS and SEVIRI data collected on Mt. Etna volcano during the November 2006 eruption are presented. The results show the importance of the ash correction on SO_2 retrieval at 8.7 μm for both MODIS and SEVIRI. The 8.7 μm SO_2 total mass corrected by the ash influence is one half and one third of the values retrieved without correction for *meanval-procedure* and *pixval-procedure*, respectively. The ash correction on the SO_2 retrieval at 7.3 μm is much less important and need only be considered for low SO_2 column abundances. The MODIS and SEVIRI ash and SO_2 retrievals result in good agreement except for the 7.3 μm SO_2 retrieval. In this case of very low SO_2 column abundance, the radiance variation could be less than the instrument sensitivity.

The results show also that the faster and simplified *meanval-procedure* underestimates the ash correction compared to the more accurate *pixval-procedure*. Such underestimation is greater for an instrument having greater ground pixel resolution, i.e. the difference between the SO_2 total mass retrieved by the two procedures is greater for MODIS than for SEVIRI.

Both correction procedures highlight that the amount of SO_2 retrieved is significantly overestimated if the effect of volcanic ash is neglected.

Acknowledgements. We thank Sergio Pugnaghi and Gabriele Gangale (University of Modena and Reggio Emilia, Italy) for helpful discussions, and the two anonymous reviewers for their editing and valuable suggestions.

Edited by: T. von Clarmann

References

Allard, P., Carbonelle, J., Dajlevic, D., Le Bronec, J., Morel, P., Robe, M. C., Maurenas, J. M., Pierret, R. F., Martins, D., Sabroux, J. C., and Zettwoog, P.: Eruptive and diffuse emission of CO_2 from Mount Etna, Nature, 351, 387–391, 1991.

Anderson, G. P., Kneizys, F. X., Chetwynd, J. H., Wang, J., Hoke, M. L., Rithman, L. S., Kimball, L. M., McClatchey, R. A., Shettle, E. P., Clought, S. A., Gallery, W. O., Abreu, L. W., and Selby, J. E. A.: FASCODE/MODTRAN/LOWTRAN: Past/Present/Future, 18th Annual Review Conference on Atmospheric Transmission Models, 6–8 June 1995.

Andronico, D., Branca, S., Calvari, S., Burton, M., Caltabiano, T., Corsaro, R. A., Del Carlo, P., Garfi, G., Lodato, L., Miraglia, L., Mur, F., Neri, M., Pecora, E., Pompilio, M., Salerno, G., and Spampinato, L.: A multi-disciplinary study of the 2002–03 Etna eruption: insights into a complex plumbing system, B. Volcanol., 67, 314–330, 2005.

Barnes, W. L., Pagano, T. S., and Salomonson, V. V.: Prelaunch characteristics of the Moderate Resolution Imaging Spectroradiometer (MODIS) on EOS-AM1, IEEE T. Geosci. Remote, 36,(4), 1088–1100, 1998.

Behncke, B. and Neri, M.: The July–August 2001 eruption of Mt. Etna (Sicily), B. Volcanol., 65, 461–476, 2003

Berk, A., Bernstein, L. S., and Robertson, D. C.: MODTRAN: A Moderate Resolution Model for LOWTRAN7, Rep. GL-TR-89-0122, Air Force Geophys. Lab., Bedford, MA, 1989.

Casadevall, T. J.: The 1989/1990 eruption of Redoubt Volcano Alaska: impacts on aircraft operations, J. Volcanol. Geoth. Res., 62(30), 301–316, 1994.

Chahine, M. T., Pagano, T. S., Aumann, H. H., et al.: AIRS: Improving weather forecasting and providing new data on greenhouse gases, B. Am. Meteorol. Soc., 87(7), 911–926, 2006.

Corradini, S., Spinetti, C., Carboni, E., Tirelli, C., Buongiorno, M. F., Pugnaghi, S., and Gangale, G.: Mt. Etna tropospheric ash retrieval and sensitivity analysis using Moderate Resolution Imaging Spectroradiometer measurements, JARS, 2, 023550, doi:10.1117/12.823215, 2008.

De Beni, E., Norini, G., and Polacci, M.: Aggiornamento dell'attivita' eruttiva (24 Novembre 2006, ore 13:00), available at: http://www.ct.ingv.it/Report/RPTVGALT20061124_1300.pdf, 2006

Ellrod, G. P., Connel, B. H., and Hillger, D. W.: Improved detection of airborne volcanic ash using multispectral infrared satellite data, J. Geophys. Res., 108(D12), 4356, doi:10.1029/2002JD002802, 2003.

Horwell, C. J. and Baxter, P. J.: The respiratory health hazards of volcanic ash: a review for volcanic risk mitigation, B. Volcanol., 69(1), 1–24, 2006.

Krotkov, N. A., Carn, S. A., Krueger, A. J., Bhartia, P. K., and Yang, K.: Band residual difference algorithm for retrieval of SO_2 from the Aura Ozone Monitoring Instrument (OMI), IEEE T. Geosci. Remote, 44(5), 1259–1266, 2006.

Pollack, J. B., Toon, O. B., and Khare, B. N.: Optical properties of some terrestrial rocks and glasses, Icarus, 19(3), 372–389, 1973.

Prata, A. J.: Observation of volcanic ash clouds using AVHRR-2 radiances, Int. J. Remote Sens., 10(4–5), 751–761, 1989a.

Prata, A. J.: Radiative transfer calculations for volcanic ash clouds, Geophys. Res. Lett., 16(11), 1293–1296, 1989b.

Prata, A. J. and Grant, I. F.: Retrieval of microphysical and morphological properties of volcanic ash plumes from satellite data: Application to Mt. Ruapehu, New Zealand, Q. J. Roy. Meteor. Soc., 127(576B), 2153–2179, 2001.

Prata, A. J., Rose, W. I., Self, S., and O'Brien, D. M.: Global, Long Term Sulphur Dioxide Measurements from TOVS Data: A New Too, for Studying Explosive Volcanism and Climate, Volcanism and the Earth Atmosphere, Geophysical Monograph 139, 75–92, 2003.

Prata, A. J. and Bernardo, C.: Retrieval of volcanic SO_2 column abundance from Atmospheric Infrared Sounder data, J. Geophys. Res., 112, D20204, doi:10.1029/2006JD007955, 2007.

Pugnaghi, S., Gangale, G., Corradini, S., and Buongiorno, M. F.: Mt. Etna sulfur dioxide flux monitoring using ASTER-TIR data and atmospheric observations, J. Volcanol. Geoth. Res., 152, 74–90, 2006.

Realmuto, V. J., Abrams, M. J., Buongiorno, M. F., and Pieri, D. C.: The use of multispectral thermal infrared image data to estimate the sulfur dioxide flux from volcanoes: a case study from Mount Etna, Sicily, July 29, 1986, J. Geophys. Res., 99(B1), 484–488, 1994.

Robock, A.: Volcanic eruptions and climate, Rev. Geophys., 38(2), 191–219, 2000.

Spinetti, C., Buongiorno, M. F., Doumaz, F., Musacchio, M., Lombardo, V., Harris, A., Steffke, A., and Amici, S.: Rapporto eruzione Etna 21–24 Novembre 2006, http://www.ct.ingv.it/Report/RPTVG200611224Roma.pdf, 2006.

Thordasson, H. and Self, S.: Atmospheric and environmental effects of the 1783–1784 Laki eruption: A review and reassessment, J. Geophys. Res., 108(D1), 4011, doi:10.1029/2001JD002042, 2003.

Waters, J. W., Froidevaux, L., Harwood, R. S., et al.: The Earth Observing System Microwave Limb Sounder (EOS MLS) on the Aura Satellite, IEEE T. Geosci. Remote, 44(5), 1075–1091, 2006.

Watson, I. M., Realmuto, V. J., Rose, W. I., Prata, A. J., Bluth, G. J. S., Gu, Y., Bader, C. E., and Yu, T.: Thermal infrared remote sensing of volcanic emissions using the moderate resolution imaging spectroradiometer, J. Volcanol. Geoth. Res., 135(1–2), 75–89, 2004.

Wen, S. and Rose, W. I.: Retrieval of sizes and total masses of particles in volcanic clouds using AVHRR bands 4 and 5, J. Geophys. Res., 99(D3), 5421–5431, 1994.

Yu, T., Rose, W. I., and Prata, A. J.: Atmospheric correction for satellite-based volcanic ash mapping and retrievals using "split window" IR data from GOES and AVHRR, J. Geophys. Res., 107(D16), 4311, doi:10.1029/2001JD000706, 2002.